CHEMISTRY OF MATERIALS

pubs.acs.org/cm

Article

Surface-Modified Group I–III–VI Semiconductor Colloidal Quantum Dots with Customized Photoluminescence and Enhanced Electronic Properties

Farzan Shabani,[⊥] Betul Canimkurbey,[⊥] Muhammad Ahmad, Savas Delikanli, Zeynep Dikmen, Furkan Isik, and Hilmi Volkan Demir*

Cite This: *Chem. Mater.* 2025, 37, 6173–6181

Read Online

ACCESS | Metrics & More | Article Recommendations | Supporting Information

ABSTRACT: Group I–III–VI semiconductor colloidal quantum dots (QDs) emerge as an exciting family of nanocrystals increasingly attractive for the next-generation solution-processed optoelectronic devices thanks to their low-cost synthesis and environmentally friendly, Cd- and Pb-free compositions. Here, a universal approach based on room-temperature surface treatment and cation exchange has been demonstrated to modify the surface and composition of $CuInS_2$, $CuInSe_2$ and $AgInS_2$ QDs. The absorption cross-section was enhanced and the emerging photoluminescence properties were finely tuned in the near-infrared region owing to great control over the size and composition of the modified QDs. While the field-effect transistors (FETs) based on the original untreated QDs exhibit *p*-type behavior and suffer from low hole mobility (μ_h), surface passivation of these QDs with an inorganic layer of S^{2-} leads to a clear switch to *n*-type behavior accompanied by a great enhancement in electron mobility (μ_e). Moreover, additional diffusion of Zn atoms into the structure heals the acceptor sites and nullifies the effect of metal vacancies and antisite defects. The FET devices based on the final modified $CuInS_2$ and $AgInS_2$ QDs demonstrate exceptionally high μ_e of 5.53 and 7.50 $cm^2\ V^{-1}\ s^{-1}$, respectively, 4 orders of magnitude higher than μ_h of the starting untreated QDs.

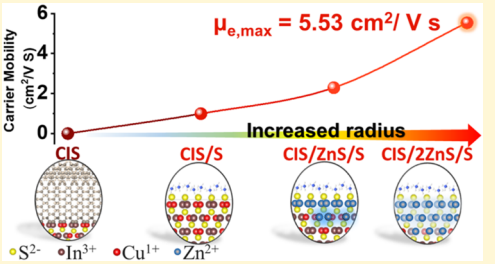

INTRODUCTION

Colloidal quantum dots (QDs) of group I–III–VI semiconductors make an exciting class of solution-processed nanocrystals (NCs) and have recently been attracting significant attention owing to their versatile synthesis and broad optoelectronic applications.[1−3] The soft crystalline structure of these QDs allows for heavy doping and alloying of their structure, which opens the door for vastly different compositions from simple ternary, such as $CuInS_2$ (CIS), $CuInSe_2$ (CISe) and $AgInS_2$ (AIS),[4−7] to Mn^{2+} and Al^{3+} doped compositions,[8−10] and further to quaternary compositions such as $CuAgInS_2$ and CuInSeS.[11,12] Characterized by their broadband, high quantum yield (PLQY) photoluminescence (PL) and extended coverage of optical absorption,[13−15] these QDs offer great potential for a vast range of optoelectronic applications.[16−26]

One effective method to tune and enhance the properties of these QDs is to coat an inorganic shell that prevents the excitons from reaching the surface.[27,28] This electronic structure, known as quasi-type-II,[29] is usually obtained through thermal decomposition of Cd or Zn precursors at relatively high temperatures, which causes the diffusion and exchange of Zn or Cd, accompanied by final shell deposition.[28,30,31] The literature on ZnS shell growth is focused on either single-pot or seed-mediated synthesis methods,[15,32] whereas implementing cation exchange was limited to the full exchange of the host atoms.[33,34] However, partial cation exchange during the shell deposition can also play a central role in the final optoelectronic properties of the QDs.[35−37]

The solution-based QDs of group I–III–VI make an excellent candidate for the next-generation flexible thin-film transistors as a potential alternative to conventional poly-crystalline silicon transistors, which require high-temperature processing.[38−40] While most of the previous electronics studies had focused on the Cd- or Pb-based devices, it was not until recently that efforts to engineer I–III–VI QDs started to grow. CIS and CISe QDs are usually known for their *p*-type behavior originating from their internal point defects due to the partial solid solution miscibility of Cu_2S and In_2S_3,[41] which produces metal vacancy defects of Cu and In and those of Cu in In (Cu_{In}) antisite defects.[42] Moreover, the surface of these QDs is covered with an unsaturated metal layer, which is known to trap charge carriers.[43] With their low hole mobility further exacerbated by the original long and bulky ligands,[44] surface

Received: March 19, 2025
Revised: July 29, 2025
Accepted: July 29, 2025
Published: August 8, 2025

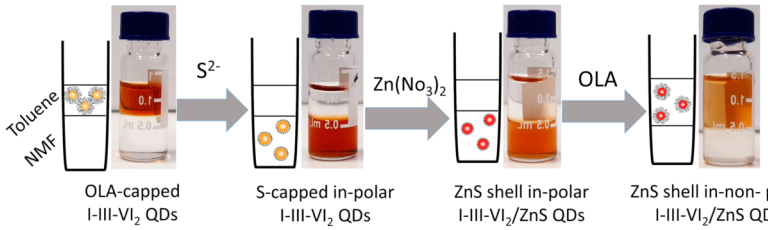

Figure 1. Schematic and the real images of the CIS QDs solution showing the synthesis steps for surface treatment of the I−III−VI QDs. First, the original QDs with long-chain OLA ligands are stably dispersed in a nonpolar solvent. The ligands are replaced with S^{2-} and the QDs are transferred to the polar solvent of NMF. The S-terminated QDs are treated with a solution of $Zn(NO_3)_2$-NMF, and at the end, the QDs are transferred back to toluene by introducing OLA.

and composition modifications are imperative to obtain QDs applicable for device applications that require high carrier mobility.

One strategy to increase the carrier mobility is to replace the long-chain ligands with shorter ones, which effectively decreases the proximity of the QDs.[45−49] In the absence of charge doping, this strategy yields higher carrier mobility, which is especially important for *p*-type QDs.[50] Shorter ligands, including halides[50,51] (Cl^-, Br^- and I^-), chalcogenides[52] (S^{2-}, Se^{2-} and Te^{2-}), pseudohalogens[53] (OCN^-, SCN^-, OH^- and SH^-), chalcogenidometallates[54] ($As_2S_3^-$) and short-chain organic ligands[55−57] (2-ethylhexane-1-thiol (EHT) and 1-octanethiol (OT), conjugated ligands) have been successfully used for a wide range of QDs, resulting in higher carrier mobility. The transport behavior and free carrier density can be tuned through composition modification with an injection of a negative or a positive charge.[42,49] The soft lattice of I−III−VI QDs allows heavy alteration and easy diffusion and exchange of atoms necessary to neutralize the acceptor sites and produce QDs with ambipolar or *n*-type behavior.[42] The post-treatment of QD thin film at elevated temperatures in the presence of an In source allows injection of extra negative charge and interdiffusion of the QDs on the film, which ultimately enhances μ_e to as high as 8.2 ± 1.8 $cm^2\ V^{-1}\ s^{-1}$ for CISe-based FETs.[41,49] Recently, Pang et al. have also demonstrated the ability to change the charge balance by implementing extra layers of S^{2-} and showed enhanced μ_e of 9.6 $cm^2\ V^{-1}\ s^{-1}$ for CISe QDs after high-temperature annealing of the QDs thin film at 350 °C.[52]

In this work, we propose and demonstrate a universal approach for the surface and composition modifications of group I−III−VI QDs based on the colloidal atomic layer deposition (c-ALD) technique and cation diffusion. Here, the original long-chain ligands were first removed, and subsequently, the surface of the QDs was passivated with the inorganic S^{2-} layer. Through the introduction of the Zn precursor, a shell of ZnS was formed on three sets of CIS, CISe and AIS QDs, which changed the PL emission peak wavelength and recombination dynamics and enhanced the absorption cross-section without changing the morphology of the QDs. This method was shown to be applicable for at least three cycles of surface treatment, in which the concentration of Zn continuously increases due to the growth and cation exchange. While the original CIS- and AIS-based devices show *p*-type behavior with poor electronic properties, the FETs based on the surface-modified QDs demonstrate *n*-type behavior with 4 orders of magnitude enhancement in their carrier mobility. This synthetic approach is especially powerful as it addresses the main causes of low carrier mobility by replacing the bulky ligands with short inorganic ligands, incorporating a surface donor layer and passivating the bulk acceptor antisite and vacancy defects through the diffusion of Zn. The final Se-free FETs exhibit electron mobility as high as 5.53 (CIS) and 7.50 (AIS) $cm^2\ V^{-1}\ s^{-1}$ with an on/off ratio of $\sim 10^5$.

EXPERIMENTAL SECTION

Sequential MS (M: Cd or Zn) Shell Treatment of CIS, AIS and CISe QDs. For the shell coating of I−III−VI QDs (the synthesis method of the core QDs is provided in the Supporting Information), first, cation precursors were prepared by dissolving 4 mmol of zinc nitrate hexahydrate or cadmium nitrate tetrahydrate in 10 mL of NMF for Zn or Cd precursors, respectively. In a typical synthesis, the original core QDs were precipitated via the addition of extra ethanol and centrifugation and redispersed in 4 mL of hexane again. The solution contains 21 optical density (OD) of the QDs at the absorption wavelengths of 538, 528, and 571 nm for CIS, AIS and CISe QDs. Here, 1 OD corresponds to the volume of sample solution that results in 1 OD absorption at the given wavelengths when 25 μL of QDs solution is diluted in 3 mL of toluene. Four mL of NMF was added to this solution, which was phase separated from hexane and then, 120 μL of $(NH_4)_2S$ was added to terminate the QDs with a sulfur layer. The solution was stirred for 5 min until all QDs were transferred from hexane to NMF, and then hexane was removed with a plastic pipet. QDs were separated from extra unreacted sulfur precursor via the addition of toluene and acetonitrile and centrifugation at 5000 rpm for 3 min, and the precipitated QDs were redispersed in NMF. The cleaning process was repeated 3 times to make sure that all of the sulfur precursor was removed. Then, 1 mL of cation precursor was added to the solution and the solution was kept under stirring. After 30 min, an extra amount of toluene and acetonitrile was added, and the solution was centrifuged at 5000 rpm for 3 min to separate the QDs. The precipitate was redispersed in NMF and cleaned two more times. At this point, the first layer of MS shell is formed. In order to continue the shell growth, we repeated the above procedure. The final product was precipitated, and 5 mL of hexane and 1 mL of OLA were added to it to passivate the surface and transfer it back to a nonpolar solvent.

RESULTS AND DISCUSSION

To treat group I−III−VI QDs with ZnS, the c-ALD technique was employed, previously reported by Talapin's group.[58] In this method, each layer of anion or cation was separately introduced to the QDs, and before the deposition of the next layer, the unreacted chemicals were removed from the reaction medium.[59,60] The method is known for its atomic precision, where reactive precursors can effectively form ionic bonds on the surface and increase the size of the QDs. The as-synthesized I−III−VI QDs capped with long-chain organic ligands are readily dispersible in nonpolar solvents. Throughout surface treatment, the ligands are first removed from the surface and replaced with short inorganic ligands that enable the QDs to be dispersed in polar solvents, in our case *N*-

https://doi.org/10.1021/acs.chemmater.5c00676
Chem. Mater. 2025, 37, 6173−6181

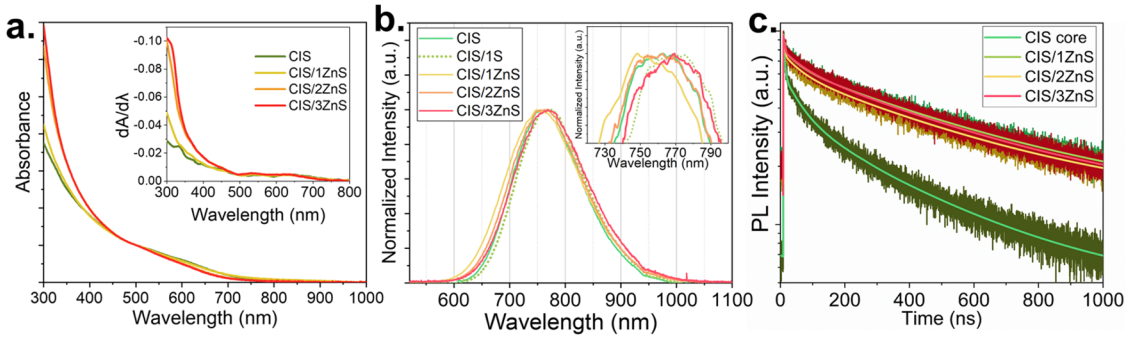

Figure 2. (a) Absorption and (b) PL spectra evolution of CIS-based QDs after a half-cycle treatment with S^{2-} and after three-time ZnS treatment. The inset in (a) presents the first derivative of the absorption spectra, and the inset in (b) displays the magnified PL peaks. (c) TRF decay curves and three-exponential fits (solid lines) of the same samples.

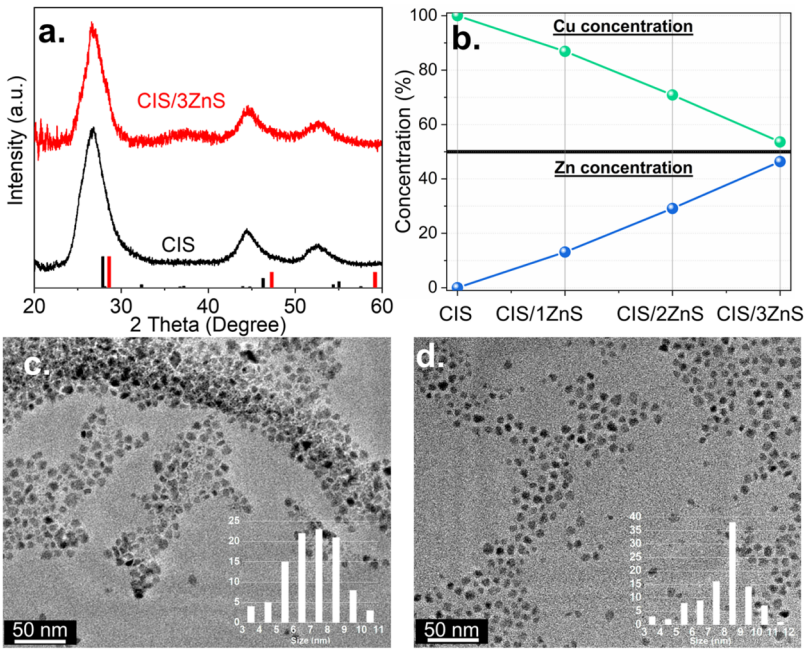

Figure 3. (a) Diffraction patterns of CIS and CIS/3ZnS QDs. Black and red bars are $CuInS_2$: ICDD 00−032−0339 and ZnS: ICDD 00−002−0564, respectively. (b) Evolution of Cu and Zn concentrations with each cycle of ZnS treatment measured via ICP-MS, in which the concentration of Zn linearly increases with the number of treatment cycles. (c) and (d) TEM image of CIS and CIS/3ZnS QDs, respectively. The insets are the size histograms of the corresponding images.

methylformamide (NMF). Figure 1 shows a step-by-step schematic and photographs of the process for ZnS-treatment of the CIS QDs. As the QDs are terminated with a metal layer, sulfur ions, in the form of ammonium sulfide with much higher affinity, can replace the original ligands and form a sulfide layer around the QDs. The interparticle electrostatic force due to the surface S^{2-} ions also gives high colloidal stability in the polar solvent. After this half-reaction, the remaining nonpolar solvent was discarded, and until the final ligation stage, the whole process was carried out in NMF. The zinc precursor (zinc nitrate-NMF) was introduced to the S-terminated QDs so that the first layer of ZnS was formed. These two steps can be subsequently used to obtain the desired number of ZnS layers where the size can be sequentially increased. At the end, the QDs were transferred back to the nonpolar solvent through ligation with the long-chain organic oleylamine (OLA) ligand.

The absorption and PL spectra of CIS QDs after three-time ZnS treatment and final ligation are presented in Figure 2a,b, respectively. The absorption onsets of the samples exhibit no obvious shift toward longer wavelengths; however, as ZnS possesses a wider bandgap and absorbs at relatively shorter wavelengths,[61] an increase in the absorption below 500 nm was observed. This increase can also be observed in the first derivative of the spectra in the inset of Figure 2a. The PL spectra show a slight blue shift after 1 ML of ZnS and continuously red-shift toward longer wavelengths. This blue shift was predictable since the Zn^{2+} ions may diffuse in the lattice and fill the vacancy defect sites or exchange with Cu and In on the surface.[62] Deposition of the extra shell layers only relaxes the confinement and induces a monotonic red shift of the PL. It is worth mentioning that after the deposition of the S^{2-} half-layer, a red shift in PL was observed due to an increase in size and relaxation of quantum confinement. The PLQY of the samples did not show much change during the three cycles of surface treatment (Table S1). This behavior can be attributed to the nature of the c-ALD method, which is prone to producing defects and possibly low PLQY, since it is generally performed at room temperature.[63]

https://doi.org/10.1021/acs.chemmater.5c00676
Chem. Mater. 2025, 37, 6173−6181

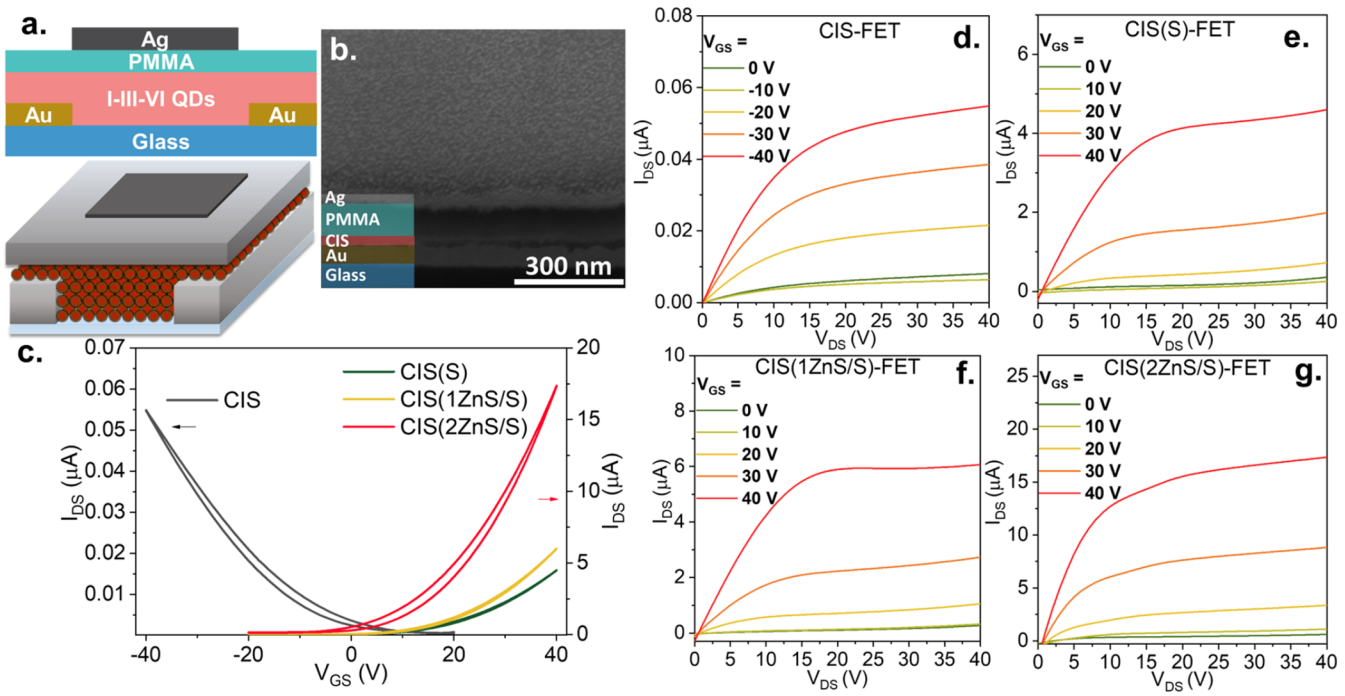

Figure 4. (a) QDs-FET device structure with top-gate/bottom-contact architecture on a glass substrate with interdigitated Au electrode. (b) Cross-sectional SEM image of the device with different layers having different contrasts. (c) Transfer characteristics (I_{DS} vs V_{GS}) of CIS-based FETs before and after surface treatment at saturation regime with V_{DS} of 20 and 40 V for original and surface-treated QDs, respectively. (d) Output characteristics (I_{DS} vs V_{DS}) of CIS-FET with long-chain OLA ligand and no surface treatment showing *p*-type behavior. (e) Output characteristics of CIS(S)-FET device after replacing the original ligands with small inorganic S^{2-} ions, showing a switch to *n*-type behavior. (f and g) Output characteristics of CIS(1ZnS/S)-FET and CIS(2ZnS/S)-FET after one and two cycles of ZnS treatment, respectively, and surface termination with S^{2-}. Both devices retained their nondegenerate *n*-type behavior.

The slight modification in the PL and absorption spectra of the samples is accompanied by a significant change in the excitonic recombination dynamics of the QDs. Figure 2c depicts the decay curves of the CIS and CIS/(1−3)ZnS QDs and their corresponding fitted lines with a three-exponential function (decay components are summarized in Table S2). The CIS core QDs have an intensity average lifetime (τ_{int}) of 351.2 ns. Upon treatment with ZnS, τ_{int} increases to 556.2 ns, 1.6 times longer than the original core. The change in the recombination dynamics points to a better passivation of the surface of the QDs, and an enlarged electron−hole distance, which increases the recombination lifetime.[64−66] The lifetime of the half-treated QDs with S^{2-} is 376.1 ns (Figure S3 and Table S3), which is close to that of the untreated QDs. Further treatment with ZnS did not induce any meaningful change in the decay rate of the QDs, indicating similar excitonic behavior.

The crystalline structure of the CIS and CIS/3ZnS QDs was examined using X-ray diffraction (XRD) measurement (Figure 3a). The lattice constant of the original chalcopyrite CIS QDs depends on the Cu/In ratio with three high-intensity peaks evident in the diffraction pattern. The zinc blende ZnS and chalcopyrite CIS crystalline structures are very similar, and the only difference originates from the bication system of the chalcopyrite, which results in the elongation of the unit cell and loss of some of the symmetries. Treatment with 3 MLs of ZnS slightly shifts the peaks to higher angles ($\Delta\theta = 0.2°$ for the first peak), closer to the diffraction peak of bulk ZnS. Moreover, the Zn diffusion into the lattice fills the vacancies, causes an exchange with Cu and In, and increases the share of zinc blende ZnS. The concentration of Zn, measured via inductively coupled plasma mass spectrometry (ICP-MS), shown in Figure 3b, demonstrates a steady increase with each surface-treatment cycle. The average radius of the QDs has increased from 6.9 ± 1.7 nm for the CIS QDs (Figure 3c) to 8.7 ± 1.5 nm for the CIS/3ZnS QDs (Figure 3d), which accounts for 26% increase in the radius or 100% in the volume of the QDs.

We examined the applicability of the method for different I−III−VI core QDs. Herein, two classes of cores were synthesized: AIS QDs, with the Cu^{+} ions replaced with Ag^{+}, and CISe QDs, in which S^{2-} ions were replaced with Se^{2-}. Both sets of QDs exhibit absorption and PL evolutions similar to the ZnS-treated CIS QDs, while a slight change in the XRD peak positions was observed, and the morphology was largely conserved (detailed in the Supporting Information). Surface treatment of CIS QDs with CdS was also demonstrated, in which the higher chemical activity of Cd and lower conduction band offset of CdS compared to ZnS resulted in a much more pronounced shift in the PL spectra with a faster increase in the Cd content (detailed in the Supporting Information).

With the ease of synthesis and high versatility for surface and structural modifications, group I−III−VI QDs are promising candidates for the next-generation electronic devices. Herein, we implemented the surface-treated QDs as the active layer in field effect transistors (FETs) and examined their electronic properties based on their structural modifications. Figure 4a demonstrates a schematic of the top-gate/bottom-contact device on a glass substrate with an interdigitated Au electrode (the fabrication process is detailed in the Supporting Information). The fabricated FETs consist of CIS QDs (CIS-FETs), CIS/S QDs (CIS(S)-FETs), CIS/ZnS/S QDs

https://doi.org/10.1021/acs.chemmater.5c00676
Chem. Mater. 2025, 37, 6173−6181

(CIS(1ZnS/S)-FETs) and CIS/2ZnS/S QDs (CIS(2ZnS/S)-FETs) as the active layer and poly(methyl methacrylate) (PMMA) layer as the gate dielectric. PMMA plays a critical role as the gate dielectric, influencing both the electrical and interfacial properties of the device. Primarily, it serves as an insulating layer that separates the gate electrode from the organic semiconductor, allowing efficient modulation of charge carriers without significant gate leakage. Owing to its moderate dielectric constant (~3.6), PMMA ensures a balance between low power consumption and sufficient gate control.[67] Additionally, PMMA provides a smooth and hydrophobic surface, which is essential for promoting the ordered growth and favorable morphology of the overlying semiconductor layer,[68] directly affecting the charge carrier mobility and reducing interface trap densities. Similarly, AIS-based FETs and CIS-based FETs treated with Cd were fabricated to compare their charge mobility performance.

The cross-sectional SEM image of an exemplary CIS-FET device in Figure 4b shows the morphology of the QDs active layer, in which a compact and crack-free CIS layer is formed. The same images of CIS(S)-FET in Figure S8 show a similar structure. For CIS-FET, the thicknesses of PMMA, QDs and Au layers are 89.0 ± 2.3, 18.8 ± 2.3 and 57.4 ± 2.7 nm, respectively, closely matching the results from the CIS(S)-FET, which has the thicknesses of 85.2 ± 1.9, 16.5 ± 1.8 and 57.7 ± 1.8 nm for PMMA, QDs and Au layers. The atomic force microscopy (AFM) image of the QDs film in Figure S9a,b confirms the formation of a smooth film with a root-mean-square roughness (R_{rms}) of 4.7 ± 2.6 nm for CIS-FET, and 5.3 ± 1.2 nm for CIS(S)-FET for a scan area of 5.0 μm^2.

The original CIS, CISe and AIS cores are capped with long-chain ligands known to reduce the charge mobility or completely inhibit the gating effect in some cases.[69] Group I−III−VI QDs exhibit both *n*-type and *p*-type behavior depending on the nature and number of the defects.[70] For example, the deficiency in the chalcopyrite or cations results in vacancy sites in the crystal structure that can play a role as donors or acceptors, respectively, while the antisite defects, such as In_{cu} (In replacing Cu in the lattice) and Cu_{In}, contribute as divalent donors and acceptors, respectively. The soft crystalline structure of I−III−VI QDs enhances the ion diffusion and chemical reactivity, critical for tailoring the charge transport behavior. It is worth mentioning that implementing different synthesis methods can affect the crystalline structure and defect density of the core QDs, which influences the electronic properties. However, even with a positive deviation of In/Cu in the composition of the core, the core-FETs still demonstrate *p*-type behavior. Here, the original cores are synthesized with the nonstochiometric precursor ratio (In/Cu = 2:1, Supporting Information) to decrease the chance of Cu_{In} defects. We have shown the applicability of ligand exchange with $(NH_4)_2S$ and consecutive cation and anion treatment, which form an inorganic ZnS or CdS layer. Knowing that surface treatment alters the nature and number of crystal defects, we examined the electronic properties of the original and surface-treated QDs. The transfer (I_{DS} vs V_{GS}) and output characteristic (I_{DS} vs V_{DS}) of CIS-FETs with varying V_{GS} from 0 to −40 V, shown in Figure 4c,d, respectively, exhibit nondegenerate *p*-type behavior of the device modulated with the gate voltage. The CIS-FET device has a rather low charge mobility of 5.46×10^{-4} $cm^2 V^{-1}s^{-1}$ and a poor on/off ratio of 0.8×10^2, similar to the previous reports in the literature.[42] The *p*-type behavior of the CIS QDs indicates the excess number of hole in comparison to the electron, which is the result of deviation from the stoichiometric composition, usually in the form of In deficiency.

The surface treatment of the QDs removes the long-chain ligands and decreases the average distance between the QDs. The replacement of these ligands with shorter S^{2-} inorganic ligands was confirmed via Fourier-transform infrared spectroscopy (FTIR) measurement shown in Figure S10, in which the peak of bending vibration at 1462 cm^{-1} corresponding to OLA[71,72] vanished after the first cycle, and the N−H stretching mode and NH_2 scissoring mode at 3300 and 1593 cm^{-1} are amplified, respectively. The complete phase transfer of the QDs from the nonpolar to polar solvent is another indication of the organic ligand removal (Figures 1 and S6). Moreover, the surface composition of the QDs was altered after sulfur and zinc treatment, which affects the stoichiometry of the QDs and the number of defects. The output characteristics of CIS(S)-FETs are shown in Figure 4e. Putting a layer of sulfur on the surface overturns the charge equilibrium and increases the density of the electrons. The unsaturated surface sites of the original QDs act as acceptors and increase the positive charge density, hence promoting the *p*-type behavior. The CIS(S)-FETs exhibit a switch from *p*-type to *n*-type due to the excessive number of electrons in the QDs. The device demonstrates an instant increase in the charge mobility to 0.99 $cm^2 V^{-1}s^{-1}$, which is already ~ 10^4 times higher than the hole mobility of CIS-FETs. The on/off ratio of the device is also enhanced by 2 orders of magnitude to 3.2×10^4 compared to CIS-FETs (Table 1). The performance of these CIS-FET devices shows no change in behavior after 21 days of measurement (Figure S11).

Table 1. Device Characteristics of FETs Based on the Original CIS QDs, (0-2 ZnS/S) and (0-2 CdS/S) Surface-Treated CIS QDs, Original AIS QDs and (0-2 ZnS/S) Surface-Treated AIS QDs[a]

FETs	μ_e/μ_h (cm^2/V s)	$I_{on/off}$	V_{Th} (V)
CIS(*)	5.46×10^{-4}	10^2	−6.4
CIS(S)	0.99	10^4	3.8
CIS(1ZnS/S)	2.29	10^5	2.7
CIS(2ZnS/S)	5.53	10^4	1.7
AIS(*)	3.44×10^{-4}	10^1	−20.0
AIS(S)	2.06	10^3	6.0
AIS(1ZnS/S)	4.57	10^4	5.6
AIS(2ZnS/S)	7.50	10^3	5.4
CIS(1CdS/S)	6.13	10^3	22.0
CIS(2CdS/S)	6.07	10^4	4.0

[a]Here, μ_e and μ_h are the average measured electron and hole mobilities, respectively. $I_{on/off}$ is the on/off current ratio, and V_{Th} is the threshold voltage. Those indicated with (*) are the hole mobility of *p*-type devices and otherwise the electron mobility of *n*-type devices.

As mentioned, the *p*-type behavior is amplified by the cation-poor, especially In-poor, stoichiometry of the QDs. The Cu_{In} antisite defects also contribute to the density of the acceptor sites.[52] On that account, if the number of cation vacancies or Cu_{In} antisite defects decreases, the electron mobility for *n*-type QDs should be enhanced. Examination of the electronic properties of CIS QDs treated with one and two layers of ZnS and terminated by S^{2-} half-layers confirms the nullification of the acceptor sites. The output characteristics of

https://doi.org/10.1021/acs.chemmater.5c00676
Chem. Mater. 2025, 37, 6173−6181

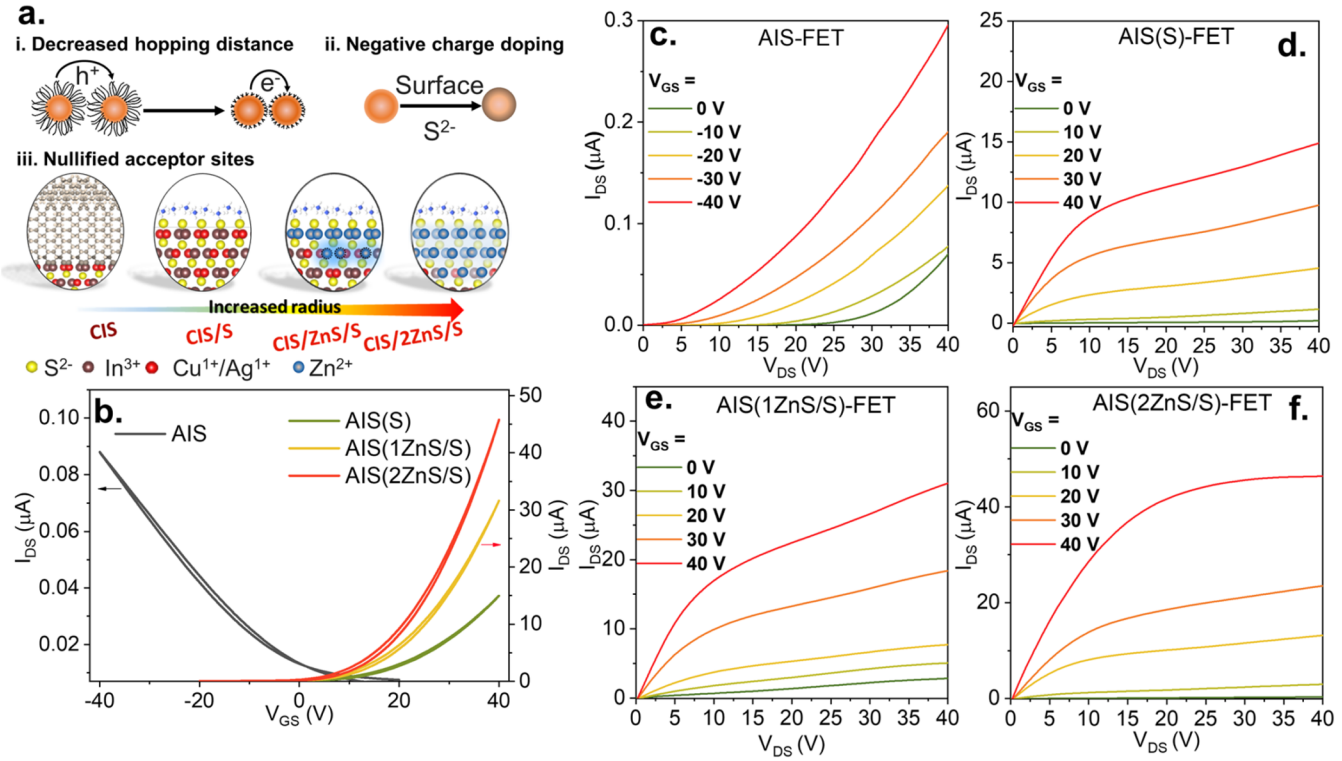

Figure 5. (a) Illustration of three main factors leading to enhancement of the carrier mobility: decreased hopping distance, negative charge doping, and nullification of the acceptor sites. (b) Transfer characteristics (I_{DS} vs V_{GS}) of AIS-based FETs before and after surface treatment at V_{DS} of 20 and 40 V, respectively. The device exhibits *p*-type behavior before surface treatment and switches to *n*-type after it. (c) Output characteristics of AIS-FET and (d) AIS(S)-FET with the OLA ligands replaced with short S^{2-} ions on the surface, which induces a switch to *n*-type behavior. (e) and (f) Output characteristics of AIS(1ZnS/S)-FET and AIS(2ZnS/S)-FET after one and two cycles of ZnS treatment, respectively, and surface termination with S^{2-}. The devices retained their *n*-type behavior while the Zn treatment enhanced the electron mobility due to the passivation of acceptor sites. To confirm the behavior, five more FETs based on the surface-treated CIS and AIS QDs were fabricated (Table S5), which confirms the gradual increase in the carrier mobility with the number of treatment cycles.

CIS(1ZnS/S)- and CIS(2ZnS/S)-FETs are shown in Figure 4f,4g, respectively. The electron mobility of the device increases after one and two cycles of ZnS treatment to 2.29 and 5.53 $cm^2\ V^{-1}\ s^{-1}$ in the saturation regime, respectively, which is more than five times higher than the CIS(S)-FETs. The increase is due to the diffusion of the Zn^{2+} ions into the lattice and replacement of V_{In} and V_{Cu} with Zn^{2+} ions or exchange of lower-valency Cu_{In} with Zn.

The origin of the charge transfer behavior and carrier mobility can be explained in terms of three factors of decreased hopping distance, negative charge doping, and nullification of the acceptor sites (Figure 5a). To better understand the applicability of surface treatment in enhancing the electronic properties of group I−III−VI QDs, FETs based on original and treated AIS QDs were fabricated. The transfer curve and the output characteristics of AIS-FETs in Figure 5b,5c, respectively, display the *p*-type behavior of the original QDs. However, unlike CIS-FETs, the AIS-FET exhibits degenerate behavior indicative of the excessive number of hole and acceptor sites. The output characteristics and transfer curve of AIS(S)-FET in Figure 5b,d, respectively, show that implementing the first S^{2-} layer causes n-doping of the device and increases carrier mobility to 2.06 $cm^2\ V^{-1}\ s^{-1}$. Treating AIS QDs with Zn (Figure 5e) enhances electron mobility by decreasing the number of the acceptor sites, as apparent from the enhanced electron mobility with further surface treatment (Figure 5f). As for AIS QDs Zn concentration increases faster than the CIS QDs (Supporting Information), the final AIS(2ZnS/S)-FETs demonstrate higher electron mobility compared to the CIS(2ZnS/S)-FETs.

Similarly, FETs based on CdS-treated CIS QDs display an initial switch from *p*-type to *n*-type behavior upon S^{2-} passivation and a secondary enhancement in μ_e with the first layer of CdS treatment due to the nullification of acceptor sites (detailed in the Supporting Information). Within the second cycle of cation treatment, the electron mobility slightly drops, suggesting no improvement in the passivation of acceptor sites. The highest μ_e for CdS-treated CIS-FETs is 6.13 $cm^2\ V^{-1}\ s^{-1}$ (improved from 2.17 $cm^2\ V^{-1}\ s^{-1}$) presented in Table 1. The experiments point to the possibility of Zn and Cd diffusion in the lattice and nullification of vacancy or antisite defects, as was shown by the chemical measurements earlier (Figures 3b and S4e), in which the cation exchange of the host ions also caused a blue shift in the PL spectra similar to a previous study.[73]

CONCLUSIONS

In conclusion, a universal strategy toward surface and composition modification of group I−III−VI QDs was developed, in which the original QDs were consecutively treated with ZnS or CdS. The optical properties, including the PL peak wavelength and recombination dynamics, can be finely tuned with ZnS treatment, while CdS treatment demonstrates a much more immense impact on the optical properties due to its lower band offset and higher Cd activity. The QDs-FETs exhibit superior electronic properties due to a

https://doi.org/10.1021/acs.chemmater.5c00676
Chem. Mater. 2025, 37, 6173−6181

combination of factors, including removal of bulky original ligands, inorganic passivation of the surface, injection of negative charge and nullification of acceptor antisite and vacancy defects after surface modification. CIS-based FETs possess a very high electron mobility of 5.53 $cm^2 V^{-1} s^{-1}$, along with an on/off ratio in the order of 10^5. The superior electronic performance of the I−III−VI-based FETs coupled with the larger absorption cross-section of the QDs can pave the way for developing high-performance photodetectors based on these QDs.

■ ASSOCIATED CONTENT

Supporting Information

The Supporting Information is available free of charge at https://pubs.acs.org/doi/10.1021/acs.chemmater.5c00676.

Synthesis and characterization methods, device fabrication and characterization, TRF decay components of ZnS-treated QDs and TRF decay curve of CIS/1S QDs, TEM images of CIS QDs, CdS Surface treatment of CIS QDs, ZnS surface treatment of AIS and CISe QDs, real images of half-layer reactions and phase transfer, cross-sectional SEM image of the device, AFM image of the device, FTIR spectra of QDs before and after ligand removal, time-dependent behavior of CIS-FET, device characteristics of extra samples, and output and transfer characteristics of CdS-treated CIS-based device (PDF)

■ AUTHOR INFORMATION

Corresponding Author

Hilmi Volkan Demir − *UNAM—Institute of Materials Science and Nanotechnology and National Nanotechnology Research Center, Department of Electrical and Electronics Engineering, Department of Physics, Bilkent University, Ankara 06800, Turkey; LUMINOUS! Center of Excellence for Semiconductor Lighting and Displays, School of Electrical and Electronic Engineering, School of Physical and Materials Sciences, School of Materials Science and Nanotechnology, Nanyang Technological University, Singapore 639798, Singapore;* orcid.org/0000-0003-1793-112X; Email: hvdemir@ntu.edu.sg, volkan@bilkent.edu.tr

Authors

Farzan Shabani − *UNAM—Institute of Materials Science and Nanotechnology and National Nanotechnology Research Center, Department of Electrical and Electronics Engineering, Department of Physics, Bilkent University, Ankara 06800, Turkey;* orcid.org/0000-0003-2174-5960

Betul Canimkurbey − *UNAM—Institute of Materials Science and Nanotechnology and National Nanotechnology Research Center, Department of Electrical and Electronics Engineering, Department of Physics, Bilkent University, Ankara 06800, Turkey; Department of Physics, Polatlı Faculty of Arts and Sciences, Ankara Hacı Bayram Veli University, Ankara 06900, Turkey*

Muhammad Ahmad − *UNAM—Institute of Materials Science and Nanotechnology and National Nanotechnology Research Center, Department of Electrical and Electronics Engineering, Department of Physics, Bilkent University, Ankara 06800, Turkey*

Savas Delikanli − *UNAM—Institute of Materials Science and Nanotechnology and National Nanotechnology Research Center, Department of Electrical and Electronics Engineering, Department of Physics, Bilkent University, Ankara 06800, Turkey; LUMINOUS! Center of Excellence for Semiconductor Lighting and Displays, School of Electrical and Electronic Engineering, School of Physical and Materials Sciences, School of Materials Science and Nanotechnology, Nanyang Technological University, Singapore 639798, Singapore;* orcid.org/0000-0002-0613-8014

Zeynep Dikmen − *UNAM—Institute of Materials Science and Nanotechnology and National Nanotechnology Research Center, Department of Electrical and Electronics Engineering, Department of Physics, Bilkent University, Ankara 06800, Turkey; Eskisehir Osmangazi University, Faculty of Engineering, Department of Biomedical Engineering, Eskisehir 26040, Turkey*

Furkan Isik − *UNAM—Institute of Materials Science and Nanotechnology and National Nanotechnology Research Center, Department of Electrical and Electronics Engineering, Department of Physics, Bilkent University, Ankara 06800, Turkey;* orcid.org/0000-0001-5881-5438

Complete contact information is available at: https://pubs.acs.org/10.1021/acs.chemmater.5c00676

Author Contributions

⊥F.S. and B.C. contributed equally to this work.

Notes

The authors declare no competing financial interest.

■ ACKNOWLEDGMENTS

The authors gratefully acknowledge financial support from the National Research Foundation, Singapore, under its NRF Investigatorship programme (NRF-NRFI10-2024-0003) and Singapore Agency for Science, Technology and Research (A*STAR) MTC program under grant number M21J9b0085. H.V.D. also acknowledges support from TUBITAK 2247-A National Leader Researchers Program (121C266) and TUBA-Turkish Academy of Sciences. B.C. acknowledges support from TUBITAK 1001 (124F030).

■ REFERENCES

(1) Berends, A. C.; Mangnus, M. J. J.; Xia, C.; Rabouw, F. T.; De Mello Donega, C. Optoelectronic Properties of Ternary I-III-VI_2 Semiconductor Nanocrystals: Bright Prospects with Elusive Origins. *J. Phys. Chem. Lett.* **2019**, *10* (7), 1600−1616.

(2) Pietryga, J. M.; Park, Y. S.; Lim, J.; Fidler, A. F.; Bae, W. K.; Brovelli, S.; Klimov, V. I. Spectroscopic and Device Aspects of Nanocrystal Quantum Dots. *Chem. Rev.* **2016**, *116* (18), 10513−10622.

(3) de Arquer, F. P. G.; Talapin, D. V.; Klimov, V. I.; Arakawa, Y.; Bayer, M.; Sargent, E. H. Semiconductor Quantum Dots: Technological Progress and Future Challenges. *Science* **2021**, *373* (6555), No. eaaz8541.

(4) Leach, A. D. P.; Macdonald, J. E. Optoelectronic Properties of $CuInS_2$ Nanocrystals and Their Origin. *J. Phys. Chem. Lett.* **2016**, *7* (3), 572−583.

(5) Sousa, V.; Gonçalves, B. F.; Franco, M.; Ziouani, Y.; González-Ballesteros, N.; Cerqueira, M. F.; Yannello, V.; Kovnir, K.; Lebedev, O. I.; Kolen'Ko, Y. V. Superstructural Ordering in Hexagonal CuInSe2 Nanoparticles. *Chem. Mater.* **2019**, *31* (1), 260−267.

(6) Feurer, T.; Carron, R.; Sevilla, G. T.; Fu, F.; Pisoni, S.; Romanyuk, Y. E.; Buecheler, S.; Tiwari, A. N. Efficiency Improvement of Near-Stoichiometric $CuInSe_2$ Solar Cells for Application in Tandem Devices. *Adv. Energy Mater.* **2019**, *9* (35), No. 1901428.

(7) Hirase, A.; Hamanaka, Y.; Kuzuya, T. Ligand-Induced Luminescence Transformation in AgInS2 Nanoparticles: From Defect

Emission to Band-Edge Emission. *J. Phys. Chem. Lett.* **2020**, *11* (10), 3969−3974.
(8) Kim, J. H.; Kim, K. H.; Yoon, S. Y.; Kim, Y.; Lee, S. H.; Kim, H. S.; Yang, H. Tunable Emission of Bluish Zn-Cu-Ga-S Quantum Dots by Mn Doping and Their Electroluminescence. *ACS Appl. Mater. Interfaces* **2019**, *11* (8), 8250−8257.
(9) Chen, J.; Li, Y.; Wang, L.; Zhou, T.; Xie, R. J. Achieving Deep-Red-to-near-Infrared Emissions in Sn-Doped Cu−In−S/ZnS Quantum Dots for Red-Enhanced White LEDs and near-Infrared LEDs. *Nanoscale* **2018**, *10* (20), 9788−9795.
(10) Rao, P.; Yao, W.; Li, Z.; Kong, L.; Zhang, W.; Li, L. Highly Stable $CuInS_2$@ZnS:Al Core@shell Quantum Dots: The Role of Aluminium Self-Passivation. *Chem. Commun.* **2015**, *51* (42), 8757−8760.
(11) Hughes, K. E.; Ostheller, S. R.; Nelson, H. D.; Gamelin, D. R. Copper's Role in the Photoluminescence of $Ag_{1-X}Cu_xInS2$ nanocrystals, from Copper-Doped $AgInS_2$ ($x \sim 0$) to $CuInS_2$ ($x = 1$). *Nano Lett.* **2019**, *19* (2), 1318−1325.
(12) Mcdaniel, H.; Koposov, A. Y.; Draguta, S.; Makarov, N. S.; Pietryga, M.; Klimov, V. I. Simple yet Versatile Synthesis of $CuInSe_xS_{2-x}$ Quantum Dots for Sunlight Harvesting. *J. Phys. Chem. C* **2014**, *118* (30), 16987−16994.
(13) Yarema, O.; Yarema, M.; Bozyigit, D.; Lin, W. M. M.; Wood, V. Independent Composition and Size Control for Highly Luminescent Indium-Rich Silver Indium Selenide Nanocrystals. *ACS Nano* **2015**, *9* (11), 11134−11142.
(14) Yarema, O.; Bozyigit, D.; Rousseau, I.; Nowack, L.; Yarema, M.; Heiss, W.; Wood, V. Highly Luminescent, Size- and Shape-Tunable Copper Indium Selenide Based Colloidal Nanocrystals. *Chem. Mater.* **2013**, *25* (18), 3753−3757.
(15) Yoon, S. Y.; Kim, J. H.; Jang, E. P.; Lee, S. H.; Jo, D. Y.; Kim, Y.; Do, Y. R.; Yang, H. Systematic and Extensive Emission Tuning of Highly Efficient Cu-In-S-Based Quantum Dots from Visible to Near Infrared. *Chem. Mater.* **2019**, *31* (7), 2627−2634.
(16) Mazzaro, R.; Vomiero, A. The Renaissance of Luminescent Solar Concentrators: The Role of Inorganic Nanomaterials. *Adv. Energy Mater.* **2018**, *8* (33), No. 1801903.
(17) Gungor, K.; Du, J.; Klimov, V. I. General Trends in the Performance of Quantum Dot Luminescent Solar Concentrators (LSCs) Revealed Using the "Effective LSC Quality Factor.". *ACS Energy Lett.* **2022**, *7* (5), 1741−1749.
(18) Jara, D. H.; Yoon, S. J.; Stamplecoskie, K. G.; Kamat, P. V. Size-Dependent Photovoltaic Performance of $CuInS_2$ Quantum Dot-Sensitized Solar Cells. *Chem. Mater.* **2014**, *26* (24), 7221−7228.
(19) Pan, Z.; Mora-Seró, I.; Shen, Q.; Zhang, H.; Li, Y.; Zhao, K.; Wang, J.; Zhong, X.; Bisquert, J. High-Efficiency "Green" Quantum Dot Solar Cells. *J. Am. Chem. Soc.* **2014**, *136* (25), 9203−9210.
(20) Kim, B.; Kim, K.; Kwon, Y.; Lee, W.; Shin, W. H.; Kim, S.; Bang, J. $CuInS_2$/CdS-Heterostructured Nanotetrapods by Seeded Growth and Their Photovoltaic Properties. *ACS Appl. Nano Mater.* **2018**, *1* (6), 2449−2454.
(21) Park, S. H.; Hong, A.; Kim, J. H.; Yang, H.; Lee, K.; Jang, H. S. Highly Bright Yellow-Green-Emitting $CuInS_2$ Colloidal Quantum Dots with Core/Shell/Shell Architecture for White Light-Emitting Diodes. *ACS Appl. Mater. Interfaces* **2015**, *7* (12), 6764−6771.
(22) Hu, G.; Sun, Y.; Zhuang, J.; Zhang, X.; Zhang, H.; Zheng, M.; Xiao, Y.; Liang, Y.; Dong, H.; Hu, H.; Lei, B.; Hu, C.; Liu, Y. Enhancement of Fluorescence Emission for Tricolor Quantum Dots Assembled in Polysiloxane toward Solar Spectrum-Simulated White Light-Emitting Devices. *Small* **2020**, *16* (1), No. 1905266.
(23) You, Y.; Tong, X.; Channa, A. I.; Li, X.; Liu, C.; Ye, H.; Wang, Z. Tailoring the Optoelectronic Properties of Eco-Friendly $CuGaS_2$/ZnSe Core/Shell Quantum Dots for Boosted Photoelectrochemical Solar Hydrogen Production. *EcoMat* **2022**, *4* (5), No. e12206.
(24) Morselli, G.; Villa, M.; Fermi, A.; Critchley, K.; Ceroni, P. Luminescent Copper Indium Sulfide (CIS) Quantum Dots for Bioimaging Applications. *Nanoscale Horiz.* **2021**, *6* (9), 676−695.
(25) Spangler, L. C.; Chu, R.; Lu, L.; Kiely, C. J.; Berger, B. W.; McIntosh, S. Enzymatic Biomineralization of Biocompatible $CuInS_2$, $(CuInZn)S_2$ and $CuInS_2$ /ZnS Core/Shell Nanocrystals for Bioimaging. *Nanoscale* **2017**, *9* (27), 9340−9351.
(26) Shen, T.; Li, F.; Zhang, Z.; Xu, L.; Qi, J. High-Performance Broadband Photodetector Based on Monolayer MoS_2 Hybridized with Environment-Friendly $CuInSe_2$ Quantum Dots. *ACS Appl. Mater. Interfaces* **2020**, *12* (49), 54927−54935.
(27) Wang, Z.; Zhang, X.; Xin, W.; Yao, D.; Liu, Y.; Zhang, L.; Liu, W.; Zhang, W.; Zheng, W.; Yang, B.; Zhang, H. Facile Synthesis of Cu-In-S/ZnS Core/Shell Quantum Dots in 1-Dodecanethiol for Efficient Light-Emitting Diodes with an External Quantum Efficiency of 7.8%. *Chem. Mater.* **2018**, *30* (24), 8939−8947.
(28) Li, L.; Pandey, A.; Werder, D. J.; Khanal, B. P.; Pietryga, J. M.; Klimov, V. I. Efficient Synthesis of Highly Luminescent Copper Indium Sulfide-Based Core/Shell Nanocrystals with Surprisingly Long-Lived Emission. *J. Am. Chem. Soc.* **2011**, *133* (5), 1176−1179.
(29) Isik, A. T.; Shabani, F.; Isik, F.; Kumar, S.; Delikanli, S.; Demir, H. V. Simultaneous Dual-Color Amplified Spontaneous Emission and Lasing from Colloidal Quantum Well Gain Media in Their Own Layered Waveguide and Cavity. *Laser Photonics Rev.* **2023**, *17* (9), No. 2300091.
(30) Portniagin, A. S.; Ning, J.; Wang, S.; Li, Z.; Sergeev, A. A.; Kershaw, S. V.; Zhong, X.; Rogach, A. L. Monodisperse $CuInS_2$/CdS and $CuInZnS_2$/CdS Core−Shell Nanorods with a Strong Near-Infrared Emission. *Adv. Opt. Mater.* **2022**, *10* (8), No. 2102590.
(31) Song, W. S.; Yang, H. Efficient White-Light-Emitting Diodes Fabricated from Highly Fluorescent Copper Indium Sulfide Core/Shell Quantum Dots. *Chem. Mater.* **2012**, *24* (10), 1961−1967.
(32) Berends, A. C.; Rabouw, F. T.; Spoor, F. C. M.; Bladt, E.; Grozema, F. C.; Houtepen, A. J.; Siebbeles, L. D. A.; De Mello Donegá, C. Radiative and Nonradiative Recombination in CuInS2 Nanocrystals and $CuInS_2$-Based Core/Shell Nanocrystals. *J. Phys. Chem. Lett.* **2016**, *7* (17), 3503−3509.
(33) Van Der Stam, W.; Bladt, E.; Rabouw, F. T.; Bals, S.; De Mello Donega, C. Near-Infrared Emitting $CuInSe_2$/$CuInS_2$ Dot Core/Rod Shell Heteronanorods by Sequential Cation Exchange. *ACS Nano* **2015**, *9* (11), 11430−11438.
(34) Portniagin, A. S.; Sergeev, A. A.; Sergeeva, K. A.; Wang, S.; Li, Z.; Ning, J.; Chan, C. C. S.; Kershaw, S. V.; Zhong, X.; Wong, K. S.; Rogach, A. L. Removing Cadmium Impurities from Cation-Exchange-Derived $CuInSe_2$/$CuInS_2$ Nanorods for Enhanced Infrared Emission and Photodetection. *Adv. Funct. Mater.* **2024**, *34*, No. 2400942.
(35) Bora, A.; Lox, J.; Hübner, R.; Weiß, N.; Jalali, H. B.; Di Stasio, F.; Steinbach, C.; Gaponik, N.; Lesnyak, V. Composition-Dependent Optical Properties of Cu-Zn-In-Se Colloidal Nanocrystals Synthesized via Cation Exchange. *Chem. Mater.* **2023**, *35* (10), 4068−4077.
(36) Lian, W.; Tu, D.; Weng, X.; Yang, K.; Li, F.; Huang, D.; Zhu, H.; Xie, Z.; Chen, X. Near-Infrared Nanophosphors Based on $CuInSe_2$ Quantum Dots with Near-Unity Photoluminescence Quantum Yield for Micro-LEDs Applications. *Adv. Mater.* **2024**, *36* (9), No. 2311011.
(37) Berends, A. C.; Van Der Stam, W.; Hofmann, J. P.; Bladt, E.; Meeldijk, J. D.; Bals, S.; De Mello Donega, C. Interplay between Surface Chemistry, Precursor Reactivity, and Temperature Determines Outcome of ZnS Shelling Reactions on $CuInS_2$ Nanocrystals. *Chem. Mater.* **2018**, *30* (7), 2400−2413.
(38) Shimoda, T.; Matsuki, Y.; Furusawa, M.; Aoki, T.; Yudasaka, I.; Tanaka, H.; Iwasawa, H.; Wang, D.; Miyasaka, M.; Takeuchi, Y. Solution-Processed Silicon Films and Transistors. *Nature* **2006**, *440* (7085), 783−786.
(39) Zhu, J.; Hersam, M. C. Assembly and Electronic Applications of Colloidal Nanomaterials. *Adv. Mater.* **2017**, *29* (4), No. 1603895.
(40) Kagan, C. R. Flexible Colloidal Nanocrystal Electronics. *Chem. Soc. Rev.* **2019**, *48* (6), 1626−1641.
(41) Draguta, S.; Mcdaniel, H.; Klimov, V. I. Tuning Carrier Mobilities and Polarity of Charge Transport in Films of $CuInSe_xS_{2-x}$ Quantum Dots. *Adv. Mater.* **2015**, *27* (10), 1701−1705.
(42) Yun, H. J.; Lim, J.; Fuhr, A. S.; Makarov, N. S.; Keene, S.; Law, M.; Pietryga, J. M.; Klimov, V. I. Charge-Transport Mechanisms in

https://doi.org/10.1021/acs.chemmater.5c00676
Chem. Mater. 2025, 37, 6173−6181

$CuInSe_xS_{2-x}$ Quantum-Dot Films. *ACS Nano* **2018**, *12* (12), 12587−12596.
(43) du Fossé, I.; Brinck, S. T.; Infante, I.; Houtepen, A. J. Role of Surface Reduction in the Formation of Traps in N-Doped II-VI Semiconductor Nanocrystals: How to Charge without Reducing the Surface. *Chem. Mater.* **2019**, *31* (12), 4575−4583.
(44) Gheshlaghi, N.; Foroutan-Barenji, S.; Erdem, O.; Altintas, Y.; Shabani, F.; Humayun, M. H.; Demir, H. V. Self-Resonant Microlasers of Colloidal Quantum Wells Constructed by Direct Deep Patterning. *Nano Lett.* **2021**, *21* (11), 4598−4605.
(45) Liu, Y.; Tolentino, J.; Gibbs, M.; Ihly, R.; Perkins, C. L.; Liu, Y.; Crawford, N.; Hemminger, J. C.; Law, M. PbSe Quantum Dot Field-Effect Transistors with Air-Stable Electron Mobilities above 7 $Cm^2 V^{-1} s^{-1}$. *Nano Lett.* **2013**, *13* (4), 1578−1587.
(46) McDaniel, H.; Fuke, N.; Makarov, N. S.; Pietryga, J. M.; Klimov, V. I. An Integrated Approach to Realizing High-Performance Liquid-Junction Quantum Dot Sensitized Solar Cells. *Nat. Commun.* **2013**, *4* (1), No. 2887.
(47) Fan, X.; Kneppe, D.; Sayevich, V.; Kleemann, H.; Tahn, A.; Leo, K.; Lesnyak, V.; Eychmüller, A. High-Performance Ultra-Short Channel Field-Effect Transistor Using Solution-Processable Colloidal Nanocrystals. *J. Phys. Chem. Lett.* **2019**, *10* (14), 4025−4031.
(48) Ibrahem, M. A.; Waris, M.; Miah, M. R.; Shabani, F.; Canimkurbey, B.; Unal, E.; Delikanli, S.; Demir, H. V. Orientation-Dependent Photoconductivity of Quasi-2D Nanocrystal Self-Assemblies: Face-Down, Edge-Up Versus Randomly Oriented Quantum Wells. *Small* **2024**, *20*, No. 2401423.
(49) Wang, H.; Butler, D. J.; Straus, D. B.; Oh, N.; Wu, F.; Guo, J.; Xue, K.; Lee, J. D.; Murray, C. B.; Kagan, C. R. Air-Stable $CuInSe_2$ Nanocrystal Transistors and Circuits via Post-Deposition Cation Exchange. *ACS Nano* **2019**, *13* (2), 2324−2333.
(50) Kim, S.; Lee, K.; Gwak, N.; Shin, S.; Seo, J.; Noh, S. H.; Kim, D.; Lee, Y.; Kong, H.; Yeo, D.; Kim, T. A.; Lee, S. Y.; Jang, J.; Oh, N. Colloidal Synthesis of *P*-Type Zn_3As_2 Nanocrystals. *Adv. Mater.* **2024**, *36* (21), No. 2310671.
(51) Choi, D.; Parmar, D. H.; Rehl, B.; Zhang, Y.; Atan, O.; Kim, G.; Xia, P.; Pina, J. M.; Li, M.; Liu, Y.; Voznyy, O.; Hoogland, S.; Sargent, E. H. Halide-Driven Synthetic Control of InSb Colloidal Quantum Dots Enables Short-Wave Infrared Photodetectors. *Adv. Mater.* **2023**, *35* (46), No. 2306147.
(52) Pang, C.; Hu, S.; Guo, C.; Wang, J.; Zou, S.; Pan, Z.; Liu, J.; Shen, L.; Bao, N.; Ning, H.; Gupta, A.; Gong, Z. High-Performance Inorganically Connected $CuInSe_2$ Nanocrystal Thin-Film Transistors and Integrated Circuits Based on the Solution Process of Colloidal Synthesis, Ligand Exchange, and Surface Treatment. *Chem. Mater.* **2021**, *33* (22), 8775−8785.
(53) Lee, J.; Yang, J.; Park, C.; Kim, J. H.; Kang, M. S. Electronic Properties of $Cu_{2-X}Se$ Nanocrystal Thin Films Treated with Short Ligand (S^{2-}, SCN^-, and Cl^-) Solutions. *J. Phys. Chem. C* **2016**, *120* (27), 14899−14905.
(54) Yakunin, S.; Dirin, D. N.; Protesescu, L.; Sytnyk, M.; Tollabimazraehno, S.; Humer, M.; Hackl, F.; Fromherz, T.; Bodnarchuk, M. I.; Kovalenko, M. V.; Heiss, W. High Infrared Photoconductivity in Films of Arsenic-Sulfide-Encapsulated Lead-Sulfide Nanocrystals. *ACS Nano* **2014**, *8* (12), 12883−12894.
(55) Zhao, C.; Zhu, C.; Xu, Z.; Ma, Q.; Yuan, F.; Li, J.; Xi, J.; Li, L.; Wang, S.; Jiao, B.; Wu, Z. Boosting Carrier Transport via Functionalized Short-Chain Conjugated Ligands Enables Efficient Green Perovskite Quantum Dot Light-Emitting Diodes. *Chem. Eng. J.* **2024**, *501*, No. 157596.
(56) Zeng, S.; Li, Z.; Tan, W.; Si, J.; Huang, Z.; Hou, X. Ultrafast Electron Transfer Dynamics Affected by Ligand Chain Length in InP/ZnS Core/Shell Quantum Dots. *J. Phys. Chem. C* **2022**, *126* (21), 9091−9098.
(57) Cao, T.; Chen, S.; Fang, F.; Tang, H.; Hao, J.; Tang, J.; Cheng, J.; Chen, W. Size Effects of 1,2-Ethanedithiol-Treated PbS Quantum Dots on Short-Wave Infrared Photodetector Hole Transport Layers. *J. Phys. Chem. Lett.* **2025**, *16*, 4607−4614.
(58) Ithurria, S.; Talapin, D. V. Colloidal Atomic Layer Deposition (c-ALD) Using Self-Limiting Reactions at Nanocrystal Surface Coupled to Phase Transfer between Polar and Nonpolar Media. *J. Am. Chem. Soc.* **2012**, *134* (45), 18585−18590.
(59) Shabani, F.; Baruj, H. D.; Yurdakul, I.; Delikanli, S.; Gheshlaghi, N.; Isik, F.; Liu, B.; Altintas, Y.; Canımkurbey, B.; Demir, H. V. Deep-Red-Emitting Colloidal Quantum Well Light-Emitting Diodes Enabled through a Complex Design of Core/Crown/Double Shell Heterostructure. *Small* **2022**, *18* (8), No. 2106115.
(60) Hu, S.; Shabani, F.; Liu, B.; Zhang, L.; Guo, M.; Lu, G.; Zhou, Z.; Wang, J.; Huang, J. C.; Min, Y.; Xue, Q.; Demir, H. V.; Liu, C. High-Performance Deep Red Colloidal Quantum Well Light-Emitting Diodes Enabled by the Understanding of Charge Dynamics. *ACS Nano* **2022**, *16* (7), 10840−10851.
(61) Bennett, E.; Greenberg, M. W.; Jordan, A. J.; Hamachi, L. S.; Banerjee, S.; Billinge, S. J. L.; Owen, J. S. Size Dependent Optical Properties and Structure of ZnS Nanocrystals Prepared from a Library of Thioureas. *Chem. Mater.* **2022**, *34* (2), 706−717.
(62) Liu, Z.; Hao, C.; Sun, Y.; Wang, J.; Dube, L.; Chen, M.; Dang, W.; Hu, J.; Li, X.; Chen, O. Rigid $CuInS_2$/ZnS Core/Shell Quantum Dots for High Performance Infrared Light-Emitting Diodes. *Nano Lett.* **2024**, *24* (17), 5342−5350.
(63) Liu, B.; Altintas, Y.; Wang, L.; Shendre, S.; Sharma, M.; Sun, H.; Mutlugun, E.; Demir, H. V. Record High External Quantum Efficiency of 19.2% Achieved in Light-Emitting Diodes of Colloidal Quantum Wells Enabled by Hot-Injection Shell Growth. *Adv. Mater.* **2020**, *32* (8), No. 1905824.
(64) Humayun, M. H.; Hernandez-Martinez, P. L.; Gheshlaghi, N.; Erdem, O.; Altintas, Y.; Shabani, F.; Demir, H. V. Near-Field Energy Transfer into Silicon Inversely Proportional to Distance Using Quasi-2D Colloidal Quantum Well Donors. *Small* **2021**, *17* (41), No. 2103524.
(65) Shabani, F.; Ahmad, M.; Kumar, S.; Delikanli, S.; Isik, F.; Bhattacharya, A.; Petrou, A.; Demir, H. V. Thermodynamic Silver Doping of Core/Shell Colloidal Quantum Wells Imparted with Paramagnetic Properties Emitting at Near-Infrared. *Chem. Mater.* **2023**, *35* (11), 4159−4170.
(66) Lim, L. J.; Zhao, X.; Tan, Z. K. Non-Toxic $CuInS_2$/ZnS Colloidal Quantum Dots for Near-Infrared Light-Emitting Diodes. *Adv. Mater.* **2023**, *35* (28), No. 2301887.
(67) Klauk, H. Organic Electronics: Materials, Manufacturing and Applications. *John Wiley & Sons* **2006**, 1−428.
(68) Rajeev, R. V.; Pillai, S.; Nunzi, J.-M.; Narayanan, U. K. N.; Vishwa Vidyapeetham Amritapuri Campus, A.. Influence of Polymer Gate Dielectric on Organic Field-Effect Transistors: Interdependence of Molecular Weight, Solvent Polarity, and Surface Energy—A Case Study with PMMA and Pentacene. *Macromol. Mater. Eng.* **2022**, *307* (3), No. 2100716.
(69) Law, M.; Luther, J. M.; Song, Q.; Hughes, B. K.; Perkins, C. L.; Nozik, A. J. Structural, Optical, and Electrical Properties of PbSe Nanocrystal Solids Treated Thermally or with Simple Amines. *J. Am. Chem. Soc.* **2008**, *130* (18), 5974−5985.
(70) Yun, H. J.; Lim, J.; Roh, J.; Neo, D. C. J.; Law, M.; Klimov, V. I. Solution-Processable Integrated CMOS Circuits Based on Colloidal $CuInSe_2$ Quantum Dots. *Nat. Commun.* **2020**, *11* (1), No. 5280.
(71) Lauth, J.; Marbach, J.; Meyer, A.; Dogan, S.; Klinke, C.; Kornowski, A.; Weller, H. Virtually Bare Nanocrystal Surfaces: Significantly Enhanced Electrical Transport in $CuInSe_2$ and $CuIn_{1-X}GaxSe_2$ Thin Films upon Ligand Exchange with Thermally Degradable 1-Ethyl-5-Thiotetrazole. *Adv. Funct. Mater.* **2014**, *24* (8), 1081−1088.
(72) Baruj, H. D.; Bozkaya, I.; Canimkurbey, B.; Isik, A. T.; Shabani, F.; Delikanli, S.; Shendre, S.; Erdem, O.; Isik, F.; Demir, H. V. Highly-Directional, Highly-Efficient Solution-Processed Light-Emitting Diodes of All-Face-Down Oriented Colloidal Quantum Well Self-Assembly. *Small* **2023**, *19*, No. 2206582.
(73) Macdonald, T. J.; Mange, Y. J.; Dewi, M.; McFadden, A.; Skinner, W. M.; Nann, T. Cation Exchange of Aqueous CuInS 2 Quantum Dots. *CrystEngComm* **2014**, *16* (40), 9455−9460.

https://doi.org/10.1021/acs.chemmater.5c00676
Chem. Mater. 2025, 37, 6173−6181